Energy 230 (2021) 120767

Contents lists available at ScienceDirect

Energy

journal homepage: www.elsevier.com/locate/energy

Process design and exergy cost analysis of a chemical looping ammonia generation system using AlN/Al_2O_3 as a nitrogen carrier

Xiaoyu Wang [a, b, 1], Mingze Su [a, 1], Haibo Zhao [a, *]

[a] State Key Laboratory of Coal Combustion, School of Energy and Power Engineering, Huazhong University of Science and Technology, Wuhan, 430074, PR China

[b] Department of Process Equipment and Control Engineering, Jianghan University, Wuhan, 430056, PR China

ARTICLE INFO

Article history:
Received 27 September 2020
Received in revised form
22 April 2021
Accepted 24 April 2021
Available online 29 April 2021

Keywords:
Chemical looping ammonia generation
Process simulation
Sensitivity analysis
Exergy analysis
Exergy cost analysis

ABSTRACT

Chemical looping ammonia generation (CLAG), in which the N_2 fixation and hydrolysis reactions occur via the circulation of nitrogen carriers, has the advantages of low-pressure, low energy consumption and high ammonia yield. Therefore, CLAG is considered as a promising alternative to conventional Haber−Bosh technology. In this work, a model for the CLAG system with a capacity of 300,000 t/a is first established. For the simulation, the N_2 fixation and hydrolysis reactors are modeled as the kinetics-based mixed flow reactor, and AlN/Al_2O_3 is used as the nitrogen carrier. The optimal operation conditions of the CLAG system are then determined by sensitivity analyses. The distribution of the exergy loss is gained from exergy analysis. The results showed that the exergy efficiency of the system reached to about 26%. Finally, exergy cost analysis is conducted to evaluate the cost formation of the system. Generally, the unit exergy cost of heat exchangers is larger than those of the other components. The distillation tower in air separation unit, the N_2 fixation reactor, and the compressor in compression and purification unit should be primarily considered in system improvement because of the significant effects of their irreversibilities on other components.

© 2021 Elsevier Ltd. All rights reserved.

1. Introduction

Ammonia is an important raw material for the production of industrial and civil chemicals, and is widely used in chemical fertilizers, refrigeration, and pharmaceutical industries [1]. Due to its high energy density, easy liquefaction, and convenient storage and transportation, ammonia is also considered as an important carrier of hydrogen [2–4]. Nowadays, over 90% of ammonia is produced through the Haber−Bosch synthesis (HBS) process [5]. However, HBS has three main limitations [5]. First, although ammonia synthesis is an exothermic process, a large amount of heat is still required to activate the nitrogen, because of its high dissociation energy [5]. Secondly, a catalyst is required to lower the activation energy. Finally, a high pressure (approximately 30 MPa) is necessary to drive the thermodynamic equilibrium of the ammonia synthesis reaction towards the ammonia generation side, and, despite this high pressure, the one-pass yield hardly exceeds 25% [5,6]. In addition, the acquisition of raw materials (hydrogen and nitrogen) for HBS consumes significant energy and release large quantities of pollutants [5].

For the above reasons, many researchers have attempted to develop new ammonia production methods with mild operating conditions, low energy consumption, and high yields. Taking advantage of the characteristics of metal nitrides (A-N) that can react with H_2O to form ammonia at low pressure, Gálvez et al. [5,7] first proposed a two-step process for ammonia production by circulating AlN/Al_2O_3 intermediates. In the first step, nitrogen is fixed by reaction with carbon and Al_2O_3 to produce AlN. In the second step, the generated AlN is hydrolyzed by steam to produce ammonia and regenerate Al_2O_3. The reaction steps are represented by R1 and R2.

$$3C + N_2 + Al_2O_3 = 2AlN + 3CO \quad \Delta H^0_{25^\circ C} = 708.1 \text{ kJ/mol} \quad \text{(R1)}$$

$$2AlN + 3H_2O = Al_2O_3 + 2NH_3 \quad \Delta H^0_{25^\circ C} = -274.1 \text{ kJ/mol} \quad \text{(R2)}$$

The proposed two-step process for ammonia production can be

* Corresponding author.
E-mail address: hzhao@mail.hust.edu.cn (H. Zhao).
[1] X. Wang and M. Su contributed equally to this work.

https://doi.org/10.1016/j.energy.2021.120767
0360-5442/© 2021 Elsevier Ltd. All rights reserved.

regarded as a special case of chemical looping [8–10]. The concept of "chemical looping combustion" was first proposed by Richter and Knoche [11], aiming to reduce exergy loss in fossil fuel combustion. The terminology of "chemical looping combustion" was first formally presented by Ishida et al. [12], with a further understanding of its essential advantages of inherent CO_2 separation and low NO_x emission. Actually, the main characteristic of chemical looping is that it splits one chemical reaction into two or multiple sub-reactions via the circulation of solid intermediate. The nitrogen carrier of AlN/Al_2O_3 in the proposed ammonia production process is just such one kind of solid intermediates. This process is, thus, called chemical looping ammonia generation (CLAG) [13,14].

With the development of CLAG, three kinds of technical route have been proposed, and they are (1) ammonia generation by the hydrolysis of metal nitrides (H_2O-CLAG) [2,5,6,13–19], (2) ammonia production via the reaction of metal nitrides with H_2 (H_2-CLAG) [20,21], and (3) ammonia formation by the hydrogenation of alkaline earth metal imides (A-NH-CLAG) [22]. In H_2O-CLAG, a metal nitride is hydrolyzed to produce ammonia and metal oxide/hydroxide. Subsequently, the metal nitride is regenerated in a N_2 fixation process. Experimental results have shown that the metal nitride/metal oxide pairs of AlN/Al_2O_3 [2,5,13–17], $Cr/Cr_2N/Cr_2O_3$ [18], $Li/Li_3N/LiOH$ [19], and Mn_5N_2/MnO [6] can be used for H_2O-CLAG. Compared with the HBS process, H_2O-CLAG has the following three advantages: the reactions proceed at low pressure without a catalyst; the raw materials (H_2O and carbon) are cheap and easily available; and the yield of ammonia is improved. However, one critical disadvantage of H_2O-CLAG is that the regeneration of the metal nitride occurs at high-temperature conditions, resulting in an energy-intensive process. H_2-CLAG consists of two steps: N_2 fixation and hydrogenation. A metal is converted to a metal nitride by N_2 fixation reaction and, then the metal nitride is reduced by H_2 to regenerate the metal and release ammonia. The main advantage of H_2-CLAG is the mild temperature conditions needed for the hydrogenation reaction. For example, the hydrogenation reactions of $Mn_6N_{2.58}$, Ca_3N_2, and Sr_2N_2 can take place at 550 °C [20], and the hydrogenation temperature of manganese nitrides could be as low as 400 °C in the presence of Li [21]. Unfortunately, the low ammonia yield and the requirement of an energy-intensive raw material (in this case, hydrogen) hinder its development. Recently, Gao et al. [22] proposed an A-NH-CLAG process utilizing alkaline earth metal hydride/imide pairs. Nitrogen is first fixed through the reaction of the alkaline earth metal hydrides with N_2 to form imides. Then, the imides are hydrogenated to produce ammonia and regenerate the metal hydrides. This process proceeds at low temperatures and low pressures, making it a promising cost-effective process.

To date, the three CLAG processes remain at the fundamental research stage, and research has mainly focused on screening of appropriate nitrogen carriers and studying the corresponding reaction processes. However, no system level study has been reported in the literature. At the system level, exergy analysis is able to detect and quantify in detail where irreversibility occurs and, thus, it is useful in the search for new improvements in energy-intensive systems. Exergy cost analysis goes a step further than exergy analysis by introducing the concept of exergy cost, and is able to analyze the process of cost formation resulting from the irreversibility in the different components of the system.

To provide guidance for experimental research and the industrialization of CLAG, we propose a CLAG system in this paper and then establish its corresponding model in Aspen Plus (schematically shown in Fig. 1). The system consists of an air separation unit (ASU), a chemical looping ammonia generation unit (abbreviated CLAG), and a compression and purification unit (CPU). Because the technical route of H_2O-CLAG has been studied in more detail (*i.e.*, the necessary reaction kinetics can be obtained from the literature),

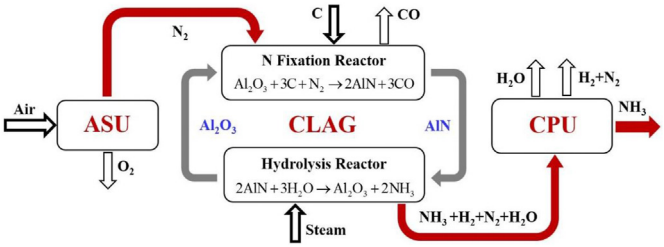

Fig. 1. Schematic of the CLAG system.

it is chosen as the object for system design and modeling in this work. The kinetics-based mixed flow reactor (MFR) model is used to simulate the hydrolysis reactor, since the equilibrium reactor model is not applicable here because the decomposition of ammonia cannot reach thermodynamic equilibrium. Based on the established model, sensitivity analyses of the key parameters of the system are subsequently conducted to determine the optimal operating conditions. Then, exergy analysis is carried out to determine the distribution of the exergy loss and the exergy efficiency of the system. Finally, exergy cost analysis is conducted to understand the cost formation process in this system.

2. Model of the CLAG system in Aspen Plus

A model of the CLAG system with a capacity of 300,000 t/a is first established in Aspen Plus, as shown in Fig. 2. The model can be simply described as follows: in the ASU, high-purity nitrogen is produced by cryogenic air separation and introduced into the CLAG unit as the reactant of the N FIXATION reactor. Then, in the CLAG unit, the mixture containing ammonia is produced by circulating the nitrogen carrier: AlN/Al_2O_3. Finally, the generated ammonia in the CLAG unit is compressed and purified in a CPU for liquid ammonia.

The following assumptions are made in the model.

1. The system is in a steady state.
2. Pressure and temperature are uniform in the reactors.
3. All equipment is operated at atmospheric pressure.
4. The energy loss in the cyclone can be ignored, and the gas–solid separation efficiency reaches 100%.
5. The gas and solid streams can be mixed completely and immediately.
6. All gases are ideal.
7. Air is taken as a mixture only containing 79 vol% N_2 and 21 vol% O_2 (*i.e.* Ar in the air is not considered).
8. The coal char used in the N_2 fixation reactor is taken as high purity carbon.

2.1. ASU model

The ASU consists of four blocks: a compressor (COMP1), a heat exchanger (HE1), a throttle valve (VALVE), and a distillation tower (TOWER1). The multistage compressor consists of four stages of compression with intermediate cooling. The isentropic efficiency and mechanical efficiency of each stage of compression are set to be 0.8 and 0.97, respectively. The final pressure of the multistage compressor was set as 6.3 bar, and the temperature of each intermediate cooling step was set to be 20 °C. According to the thermodynamic properties of oxygen and nitrogen, the outlet of the distillation column is gaseous nitrogen and liquid oxygen. The concentration of gaseous nitrogen is set as 99 mol.% (some

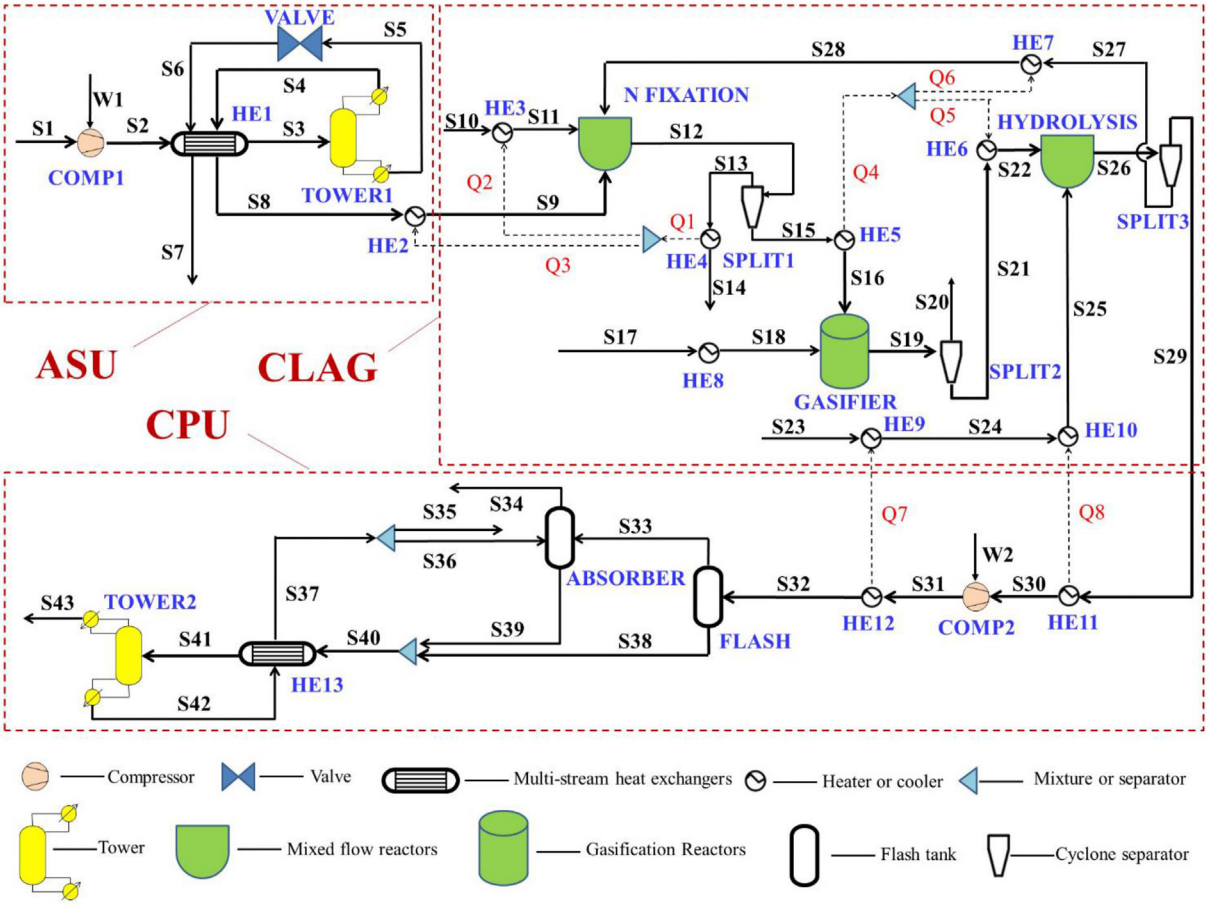

Fig. 2. Schematic of the CLAG system modeled in Aspen Plus.

remaining oxygen will be removed by carbon in the N FIXATION reactor in practice, and it will not affect R1 because the reaction between carbon and oxygen can proceed more rapidly than R1). Before the introduction into the CLAG unit for further processing, the produced N_2 is preheated in HE1. A brief descriptions of the blocks used here are shown in Table S1 in Supplementary material (SM).

2.2. CLAG unit model

The high-purity nitrogen produced in the ASU is further heated in HE2, and, eventually, it (S9) is fed into the CLAG unit. The CLAG unit consists of an N FIXATION reactor, hydrolysis reactor, gasification reactor, three cyclone separators, seven heaters, and two coolers. Table S2 in SM summarizes the descriptions of the blocks used in this unit.

In the CLAG unit, the carbon preheated in HE3 and high-purity nitrogen are first introduced into the N FIXATION reactor. In this unit, the circulated Al_2O_3 is converted to AlN by reaction with carbon and nitrogen. Through this conversion, nitrogen is fixed to the solid nitrogen carriers. Subsequently, the products of the N FIXATION reactor flow into the cyclone, SPLIT1, for gas–solid separation. The separated gas, S13, is collected for further utilization after being cooled by the cooler, HE4. The separated solid mixture of carbon residue, Al_2O_3, and AlN (S15) is cooled to 750 °C by the cooler, HE5, before it is fed into the GASIFIER reactor. To remove excess carbon, in the GASIFIER reactor, the carbon is gasified by the steam generated in HE8 to form CO and H_2. It should be noted that the hydrolysis of AlN barely occurs at 750 °C [13], so the hydrolysis of AlN is not considered in the GASIFIER reactor. The outlet stream of the GASIFIER reactor is introduced into the cyclone, SPLIT2, and divided into two branches: a gas mixture containing CO, H_2, and H_2O (S20), and a solid mixture containing Al_2O_3 and AlN (S21). Because the amounts of valuable species in S20 (as will be discussed in Section 3.4) are small, it is not worth recycling by investing additional equipment in practice. Therefore, after being combusted, the stream of S20 is discharged into the atmosphere. The solid mixture flows into the HYDROLYSIS reactor to react with steam and is heated gradually by heaters HE9 and HE10 to produce ammonia and regenerate Al_2O_3 simultaneously. As ammonia can be decomposed under the condition of the hydrolysis reaction, the decomposition of ammonia should also be considered in HYDROLYSIS. The outlet stream, S26, of HYDROLYSIS is then separated into a solid stream, S27, and a gas stream, S29, by a cyclone, SPLIT3. The solid stream circulates back into the N FIXATION reactor for the next cycle, and the gas stream containing NH_3 is cooled by cooler HE11 to feed the compression and purification unit.

2.3. CPU model

The aim of the CPU is to separate and concentrate NH_3 from the outlet gas of the hydrolysis reactor. This unit consists of two coolers (HE11/HE12), a compressor (COMP2), a flash tank (FLASH), an absorber (ABSORBER), a heat exchange (HE13), and an ammonia distillation tower (TOWER2). Table S3 in SM shows the brief descriptions of the blocks used in the CPU.

The mixture in stream S29 containing NH_3 from the CLAG unit is introduced into this unit. First, it is cooled in HE11, and, then, the outlet stream of HE11 is compressed to 21.6 bar (323.5 °C) by the multistage compressor, COMP2. The outlet stream of the compressor is further cooled by HE12 before it is conveyed to FLASH to separate the gas and liquid. The outlet gas of FLASH containing N_2, H_2, and a little NH_3 is introduced into ABSORBER. At this stage, ammonia is absorbed by the liquid water in S36. The outlet gas of ABSORBER is a mixture of nitrogen and high-concentration hydrogen, whereas the bottom liquid of ABSORBER is dilute ammonia water. Then, the dilute ammonia water is mixed with the bottom liquid of the FLASH. Before the mixture stream containing ammonia water enters TOWER2, it is heated to 140 °C by the bottom stream of the TOWER2 in HE13. In TOWER2, the stream of ammonia water is in direct countercurrent contact with steam from the bottom of the tower. Thus, the stream of ammonia water is heated. At high temperatures, ammonia is released from the ammonia water, and eventually, ammonia with a concentration of 99.9 mol.% is attained.

2.4. Heat integration and input/output streams of the CLAG system

To improve the energy utilization efficiency of the whole CLAG system, the heat stream of Q1 from HE4 is introduced into HE2 and HE3 to heat the feeding stream of the N FIXATION reactor. The heat streams of Q4, Q7, and Q8 from HE5, HE12, and HE11 are supplied to HE6/HE7, HE9, and HE10, respectively.

Tables 1 and 2 show the components and molar fractions of the input and output streams of the system, respectively. From the two tables, it can be seen that the raw materials of the system are cheap and easily available. Moreover, all the output streams of the system (except S35 and S20) are useful and can be considered as products. For example, S43 is the main product (concentrated NH_3), S7 and S14 are high-purity O_2 (The O_2 may not be pure enough in actual process as the argon in air was not considered in the current analysis) and CO, respectively, and S34 is high-value H_2.

3. Simulation results and analysis

3.1. Reactor model for CLAG

The reactor model RGIBBS is not applicable for modeling the hydrolysis reactor because, in practice, the overall hydrolysis process cannot reach its thermodynamic equilibrium (*i.e.*, ammonia decomposes nearly completely) in most cases. That is to say, the decomposition rate of ammonia is slower than its generation rate under such conditions, and the ammonia generated by AlN hydrolysis discharges from the reactor rapidly before its complete decomposition. As the reaction kinetics of N_2 fixation, AlN hydrolysis, and NH_3 decomposition reactions can be obtained from the literature [13,15,23], the kinetics-based MFR model is used to simulate the N_2 fixation and hydrolysis reactors.

Galvez et al. [13,15] experimentally tested the reaction rates of N_2 fixation and AlN hydrolysis reactions by thermogravimetric analysis (TGA). They found that the shrinking core model is suitable for the reaction rate description, and finally gave the reaction kinetics of the above two reactions. However, in order to use this kinetics in Aspen Plus, some transformations are needed. Taking the kinetics of the hydrolysis reaction as an example, the transformation is as follows.

The original form of the reaction kinetics given by Galvez et al. [13] is

$$1-(1-X_{\mathrm{HYDRO}})^{1/3}=3.3\times10^{5}e^{-186300/RT}(P_{\mathrm{H_2O}}/P_{\mathrm{atm}})t \tag{1}$$

where X_{HYDRO} represents the conversion of AlN in the hydrolysis reaction, R is the universal gas constant, T is the temperature, $P_{\mathrm{H_2O}}$ and P_{atm} represent the partial pressure of steam and the atmospheric pressure, respectively, and t is time. The integral form shown in Eq. (1) can be converted to the differential form as,

$$\frac{dX_{\mathrm{HYDRO}}}{dt}=3\times3.3\times10^{5}e^{-186300/RT}(P_{\mathrm{H_2O}}/P_{\mathrm{atm}})(1-X_{\mathrm{HYDRO}})^{2/3} \tag{2}$$

Substituting the ideal gas equation into Eq. (2), we obtain

$$\frac{dX_{\mathrm{HYDRO}}}{dt}=\frac{3\times3.3\times10^{5}\cdot8.314}{101325}Te^{-186300/RT}C_{\mathrm{H_2O}}(1-X_{\mathrm{HYDRO}})^{2/3} \tag{3}$$

where $C_{\mathrm{H_2O}}$ is the molar concentration of steam. It should be noted that the units of $\frac{dX_{\mathrm{HYDRO}}}{dt}$ and $C_{\mathrm{H_2O}}$ in Eq. (3) are [min^{-1}] and [mol/m^3], respectively. However, their default units in Aspen Plus are [s^{-1}] and [$kmol/m^3$]. By unit conversion, Eq. (3) becomes:

$$\frac{dX_{\mathrm{HYDRO}}}{dt}=1.354\times10^{3}Te^{-186300/RT}C_{\mathrm{H_2O}}(1-X_{\mathrm{HYDRO}})^{2/3} \tag{4}$$

With respect to the process simulation on the reactor scale, X_{HYDRO} can (only) be represented by $1-\frac{C_{\mathrm{AlN}}}{C_{\mathrm{AlN}}+2C_{\mathrm{Al_2O_3}}}$, where C_{AlN} and $C_{\mathrm{Al_2N_3}}$ represent the mole concentrations of AlN and Al_2O_3 based on the unit volume of the hydrolysis reactor ($kmol/m^3$). In fact, the above definition is the conversion of Al element in the hydrolysis reactor, but it is just equal to the conversion of AlN. As C_{AlN} can also represent the mole concentration of Al element that has not been converted in the hydrolysis reactor, while the total mole concentration of Al element in the hydrolysis reactor can be represented by $C_{\mathrm{AlN}}+2C_{\mathrm{Al_2N_3}}$. Substituting it into Eq. (4) results in Eq. (5).

$$-\frac{dC_{\mathrm{AlN}}}{dt}=1.354\times10^{3}Te^{-186300/RT}C_{\mathrm{H_2O}}\frac{C_{\mathrm{AlN}}^{2/3}}{(C_{\mathrm{AlN}}+2C_{\mathrm{Al_2O_3}})^{-1/3}} \tag{5}$$

Note that $C_{\mathrm{AlN}}+2C_{\mathrm{Al_2O_3}}$ does not change as the hydrolysis conversion of AlN proceeds. The reaction rate of R2 is finally given as

$$r_{\mathrm{R2}}=676.9Te^{-186300/RT}\frac{C_{\mathrm{H_2O}}C_{\mathrm{AlN}}^{2/3}}{(C_{\mathrm{AlN}}+2C_{\mathrm{Al_2O_3}})^{-1/3}} \tag{6}$$

Obviously, the reaction rate cannot be simply expressed in the power law form. Fortunately, Aspen Plus provides the specification method of Langmuir–Hinshelwood–Hougen–Watson (LHHW) reaction kinetics, as follows:

$$r=\frac{kT^{n}e^{-E_a/RT}[K_1(\Pi C_i^{\nu_i})-K_2(\Pi C_j^{\nu_j})]}{[\sum K_m(\Pi C_n^{\nu_n})]^{l}} \tag{7}$$

Comparing Eq. (6) with Eq. (7), it can be found that the LHHW

Table 1
Components and molar fractions of the input streams.

Stream	S1	S10	S17	S23
Component	N_2/O_2	C	H_2O	H_2O
Molar fraction	0.790/0.210	1.000	1.000	1.000
Mole flow, kmol/h	2227.00	4300.00	50.00	20000.00

Table 2
Main components and molar fractions of the output streams.

Stream	S7	S14	S20	S34	S35	S43
Component	O_2	CO/N_2	$H_2/CO/H_2O$	$H_2O/N_{2//}H_2$	H_2O	H_2O/NH_3
Molar fraction	1.000	0.924/0.071	0.085/0.085/0.830	0.025/0.244/0.731	1.000	0.001/0.999
Mole flow, kmol/h	442.35	4648.24	54.62	841.60	15684.68	2452.35

reaction kinetics can be used to express the reaction rate shown in Eq. (6) by setting $k = 676.9$, $n = 1$, $E_a = 186300$, $K_1 = 1$, $K_2 = 0$, $l = -1/3$, $\Pi C_i^{\nu_i} = C_{H_2O} C_{AlN}^{2/3}$, and $\sum K_m(\Pi C_n^{\nu_n}) = C_{AlN} + 2C_{Al_2O_3}$.

The kinetic transformation for the N_2 fixation reaction, R1, can be carried out similarly. Only the original form and the final form are given here in Eqs. (8) and (9).

$$1 - (1 - X_{N\_FIX})^{1/3} = 3.98 \times 10^9 e^{-435700/RT}(P_{N_2} / P_{atm})t \quad (8)$$

$$r_{R1} = 1.633 \times 10^7 T e^{-435700/RT} \frac{C_{N_2} C_{Al_2O_3}^{2/3}}{(C_{Al_2O_3} + 0.5C_{AlN})^{-1/3}} \quad (9)$$

The conversion of AlN should be understood from two different scales, *i.e.*, the particle scale and the reactor scale. In Eq. (1), X_{HYDRO} is the conversion at the particle scale, that is to say, it represents the conversion of a single particle. While in Eq. (6), X_{HYDRO} is the conversion at the reactor scale, and its definition is $X_{HYDRO} = 1 - C_{AlN}/(C_{AlN} + 2C_{Al_2N_3})$. When the particles in the reactor are considered to be identical (although it is almost impossible), the above two kinds of conversion are identical. The reason that we conduct such a scale transformation is: in the reactor scale simulation, one can hardly get the conversion at the particle scale directly. Actually, such scale transformation is a common practice in reactor scale simulations, and it can be found in many previous studies [24,25].

The kinetic parameters for the decomposition reaction of ammonia are determined by fitting the simulation results of the detailed reaction mechanism of CO/H_2 with 32 components and 173 reactions. This detailed mechanism was developed by Ranzi et al. [23], which not only included the reaction path for CO/H_2 but also the conversion path of the nitrogen component. The kinetics is fitted as follows: First, a perfectly stirred reactor model with inlet and outlet was constructed in CHEMKIN. Then, the detailed reaction mechanism described above was imported. Subsequently, simulations were conducted for 24 cases at four different temperatures (927 °C, 1027 °C, 1127 °C, and 1327 °C) and six different inlet concentrations of NH_3 (5%, 10%, 20%, 40%, 70%, and 90%). In the simulation, the residence time of the reactor was set to ensure little difference in NH_3 concentration between the inlet and outlet of the reactor. This means that NH_3 is decomposed at this concentration condition, which is similar to that of the inlet. The decomposition rate of NH_3 in each case was calculated based on the simulation results. Finally, the kinetics of NH_3 decomposition was determined by Arrhenius fitting, as:

$$r_{NH3\_DEC} = 2.16 \times 10^{12} e^{-392545/RT} C_{NH_3}^{0.953} \quad (10)$$

Obviously, the NH_3 decomposition can be specified as a POWERLAW reaction in Aspen Plus.

3.2. Validation of reaction kinetics in simulation

To validate the reaction kinetics used in the simulation, a plug flow reactor (PFR) model was used to calculate the solid conversion vs. reaction time. The PFR model instead of the MFR model was used for kinetic validation because it is possible to reproduce the isothermal TGA experimental results by setting appropriate reaction conditions in the PFR simulation, which however is not possible in the MFR simulation. This is because the PFR is a one-dimensional reactor, but the MFR is a zero-dimensional reactor.

The above-mentioned appropriate reaction conditions are discussed further. First, the temperature of the PFR should be the same as the experimental one, and the energy equation should not be solved for the PFR to obtain an isothermal result. Secondly, in TGA, the gaseous reactants are supplied continuously in excess compared to the solid reactants. Therefore, it is reasonable to consider that the solid reactants are converted under an unchanged atmosphere. However, in PFR, the gaseous and solid reactants are continuously consumed along with the reactor length after introduction. To achieve reaction conditions for the solid reactants in PFR similar to those in TGA, the gaseous reactants at the reactor inlet should be in excess. Only in this case, the gas composition can be considered unchanged both spatially and temporally.

Fig. 3 shows a comparison between the simulation results and experimental results [13,15]. The times required for 30% conversion of Al_2O_3 and AlN from the simulation and experiment are shown in Table S4 and Table S5 in SM. It can be seen that the simulation results are in good agreement with the experimental ones. The errors could be attributed to the small differences in the concentration conditions of gaseous reactants.

3.3. Sensitivity analyses

For optimal operation of the CLAG system, sensitivity analyses are carried out based on the above system model. The following issues are discussed: the effects of the N_2 fixation reactor temperature and the air flow rate on the outlet volume fraction of CO in the N_2 fixation reactor and the ammonia yield of the system. Meanwhile, the effects of the hydrolysis reactor temperature and the H_2O flow rate on the outlet volume fractions of hydrogen and ammonia in the hydrolysis reactor and the ammonia yield of the system. In each sensitivity analysis, only the corresponding parameter changes, while the others remain unchanged. Before the sensitivity analyses, the general scopes of the studied parameters are determined according to the ammonia production capacity as follows: the air flow rate ranges from 1500 to 4000 kmol/h; the H_2O flow rate ranges from 5000 to 40000 kmol/h; the N_2 fixation reactor temperature is set as 1500, 1600, 1700, 1800, or 1900 °C; and the hydrolysis reactor temperature is 900, 1000, or 1100 °C.

3.3.1. Effect of N_2 fixation reactor temperature

The outlet gas of the N_2 fixation reactor, which consists of CO and N_2, could be used as gas fuel or raw material for chemical synthesis. Therefore, not only the NH_3 yield of the system but also the CO concentration at the outlet of the N_2 fixation reactor should be carefully considered. Fig. 4 shows the simulation results of the five different temperatures. It can be observed that the CO concentration and ammonia yield increase with temperature, especially from 1500 to 1700 °C. Theoretically, a high temperature is helpful to facilitating the reaction rate and the product yield of the endothermic reaction thermodynamically. Therefore, it is easy to understand why the concentrations of CO and AlN at the outlet of

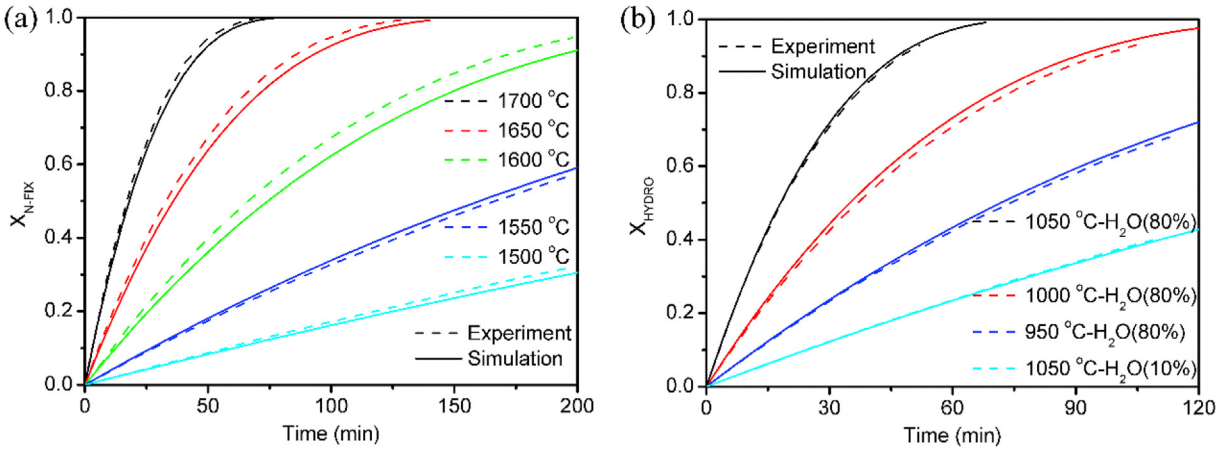

Fig. 3. Comparison of the conversion of Al_2O_3 vs. time in the N_2 fixation reaction (a) and the conversion of AlN vs. time in the hydrolysis reaction (b) for kinetics validation.

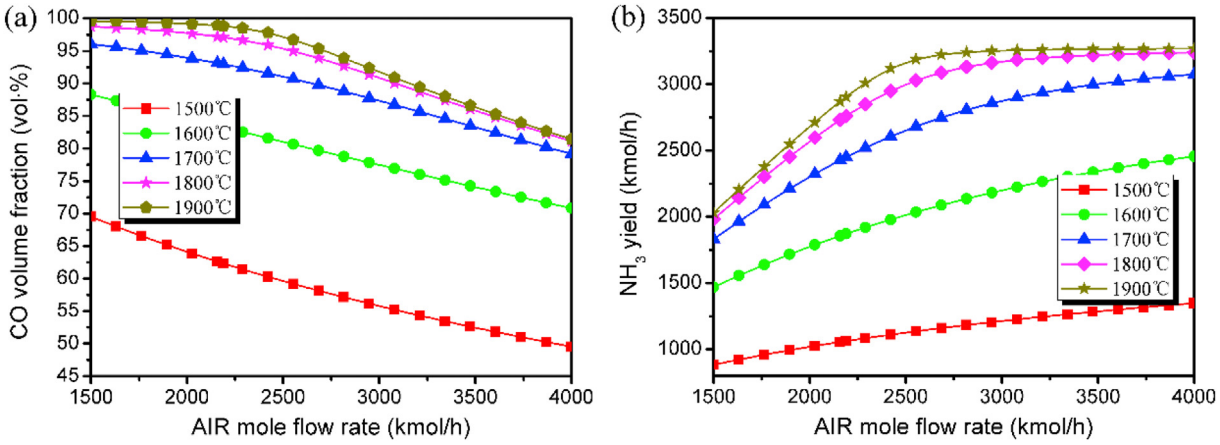

Fig. 4. CO concentration at the outlet of the N_2 fixation reactor (a) and the NH_3 yield of the system (b) as a function of the air flow rate at different temperatures of the N_2 fixation reactor.

the N_2 fixation reactor increase with temperature. The increasing AlN concentration accelerates the reaction rate in the hydrolysis reactor, resulting in a high NH_3 yield. To achieve a balance of technical feasibility and system performance, 1700 °C is used as the N_2 fixation reactor temperature.

3.3.2. *Effect of air flow rate*

The simulation results of different air flow rates are also shown in Fig. 4. It can be seen that the CO concentration initially decreases slowly, and then decreases sharply with the increase of air flow rate. The reason is that when the air flow rate is low, the amount of N_2 produced by ASU is lower than the N_2 fixation capacity of the N_2 fixation reactor. In this case, most of the N_2 produced can be fixed, so the amount of N_2 at the outlet of the N_2 fixation reactor does not increase significantly. However, when the air flow rate is high, the amount of N_2 produced is larger than the N_2 fixation capacity. Thus, a large amount of unfixed N_2 flows out of the N_2 fixation reactor, which dilutes the outlet CO concentration. The NH_3 yield increases rapidly with the increase of air flow rate initially and then remains nearly unchanged. In fact, the NH_3 yield is positively related to the AlN yield in the N_2 fixation reactor. Similarly, when the air flow rate is low, the AlN yield increases with the increase of air flow rate. However, being limited by the amount of nitrogen carriers, the AlN yield does not always increase with the air flow rate. Based on the above analyses and the requirement of ammonia production capacity, the optimal air flow rate is determined to be 2227 kmol/h in this work.

3.3.3. *Effect of hydrolysis reactor temperature*

AlN hydrolysis and ammonia decomposition occur simultaneously in the hydrolysis reactor. It has been found experimentally that AlN hydrolysis does not occur until the temperature is higher than 900 °C [13]. On the other hand, high temperatures can accelerate ammonia decomposition, which results in a decrease in ammonia yield. Therefore, it is crucial to determine the hydrolysis reactor temperature by considering the above two opposing factors. In this work, three temperatures (900 °C, 1000 °C, and 1100 °C) were selected for investigation, and the results are shown in Fig. 5.

The outlet concentration of H_2 always increases with increase in temperature. Whereas, after an initial increase period, the outlet concentration of NH_3 and its yield decrease rapidly with the increase of temperature. Because H_2 is produced by the decomposition of NH_3 (where a high temperature is beneficial to the increase of the decomposition rate), and the concentration of H_2 increases with temperature. Ammonia is generated by AlN hydrolysis, and is consumed by NH_3 decomposition. In the initial period (900–1000 °C), as limited by the low concentration of NH_3, the increase in the decomposition rate is lower than that of the hydrolysis rate with the increase of hydrolysis temperature. The concentration of NH_3, thus, increases. However, after a critical

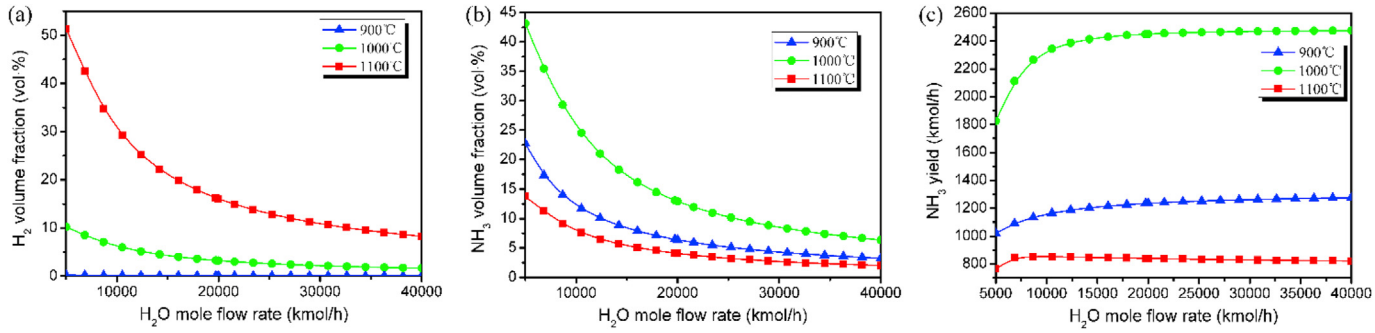

Fig. 5. Outlet concentrations of H_2 (a) and NH_3 (b) of the hydrolysis reactor and NH_3 yield of the system (c) as a function of the H_2O flow rate at different temperatures of the hydrolysis reactor.

hydrolysis temperature (i.e., 1000 °C), the decomposition rate increases more rapidly with the hydrolysis temperature because it has a larger apparent activation energy. As a result, the concentration of NH_3, as well as its yield, decreases.

Through the above analyses, we determined that the ammonia concentration and its yield reach their maxima when the hydrolysis reactor is operated at 1000 °C. Therefore, the optimal temperature of the hydrolysis reactor was determined to be 1000 °C.

3.3.4. *Effect of H_2O flow rate*

Fig. 5 shows that the outlet concentrations of H_2 and NH_3 decrease and the NH_3 yield increases with increase in H_2O flow rate. NH_3 is produced by the reaction of AlN with H_2O, so the increase in H_2O flow rate contributes to NH_3 generation. However, the dilution effect of the unreacted H_2O on the concentrations of H_2 and NH_3 is more significant. Although the excess H_2O in H_2 and NH_3 can be easily removed by condensation, it is still undesirable because it increases the energy consumption of the whole system. To obtain a high NH_3 yield without reducing the concentrations of H_2 and NH_3 too much, the optimal H_2O flow rate is determined to be 20000 kmol/h.

3.4. *Exergy analysis*

Exergy focuses not only on the quantity but also on the quality of energy. The exergy analysis is usually used to determine the magnitudes, locations, and types of exergy losses occurring in the system [26,27]. In the present analysis, the environmental model shown in Table 3 (with a reference temperature of 25 °C and pressure of 1.013 bar) was used for the exergy calculation.

The kinetic exergy and potential exergy are ignored because their changes have negligible effects on the results of the total exergy change in such a thermodynamic system. Therefore, the total exergy of each stream, which consists of the physical exergy (e^{ph}) and chemical exergy (e^{ch}), can be determined as

Table 3
Definition of environmental model.

Component	Mole fraction	Chemical exergy, kJ/kmol
Al_2O_3		0
C		410530
N_2	0.7567	670
AlN		501527.5
CO		275350
$H_2O(l)$		0
NH_3		336690
H_2		235220
O_2	0.2035	3930

$$e = e^{ph} + e^{ch} \tag{11}$$

the method used to calculate the physical exergy and chemical exergy has been described in detail in our previous work [26].

For the system operated under the optimal conditions, the parameters of each stream in the system are tabulated in Table S6, and the exergy of each stream is shown in Table 4. The following definition of the exergy efficiency was chosen to evaluate the exergy efficiency of the system.

$$\eta = \frac{E_P}{E_F} = 1 - \frac{E_{in} + E_{ex}}{E_F} \tag{12}$$

Here, E_F and E_P represent the fuel exergy and product exergy, respectively. The fuel exergy is the exergy absorbed by the system from the environment, which includes the exergy of not only the inlet stream but also the heat flow entering the system. Generally, there are two kinds of exergy loss: the internal exergy loss, E_{in}, and the external exergy loss, E_{ex}. The internal exergy loss is caused by the irreversibility in the system, and it reflects the thermodynamic limitations of the technique. The external exergy loss is the exergy discharged into the environment with heat and byproduct emissions. As shown in Table 2, there are six streams discharged into the environment, and they are S7 (high-purity O_2 from ASU, 442.35 kmol/h), S14 (concentrated CO from the N_2 fixation reactor, 92.4% and 4648.24 kmol/h), S20 (lower concentration of syngas from the gasifier, 17.0% and 54.62 kmol/h), S34 (concentrated H_2 from CPU, 73.1% and 841.6 kmol/h), S35 (liquid water, 15684.68 kmol/h), and S43 (high-purity NH_3 from CPU, 99.9% and 2452.35 kmol/h). The stream S43 is the product stream containing high-concentration of liquid ammonia, and streams S7, S14, and S34 can also be considered as product streams because they contain high concentrations of O_2, CO, or H_2, which can be used for other industries. Although the syngas in S20 can be concentrated by steam condensation, stream S20 is still not considered as a product stream because the amount of valuable species in S20 is so small that it is not worth recycling. Therefore, the external exergy loss consists of two parts in this system: one is the exergy of streams S20 and S35, and the other one is the exergy discharged by heat dissipation in TOWER1, TOWER2, and HYDROLYSIS. The internal exergy loss is shown separately for the three units in Figs. 6–8.

Fig. 6 shows the internal exergy loss of each part of the ASU. The largest exergy loss is located in the distillation tower. This is because the energy penalty for phase transformation occurring in the kettle reboiler and overhead condenser of the distillation tower is much larger than that for pressurization and heat transfer in the compressor and heat exchanger. The heat exchanger, HE1, also has a relatively large exergy loss. This is mainly because of the large temperature difference between the inlet and outlet streams.

Table 4
Physical, chemical, and total stream exergy.

Stream	Physical exergy (kW)	Chemical exergy (kW)	Stream exergy (kW)	Stream	Physical exergy (kW)	Chemical exergy (kW)	Stream exergy (kW)
S1	0.00	49.86	49.86	S23	0.00	0.00	0.00
S2	2818.96	49.86	2868.82	S24	52204.88	0.00	52204.88
S3	5224.72	49.86	5274.58	S25	154709.50	0.00	154709.50
S4	3014.76	263.21	3277.97	S27	402852.32	2918112.98	3320965.31
S5	2192.40	481.66	2674.06	S28	987983.39	2918104.59	3906087.98
S6	2158.46	481.66	2640.12	S29	154071.51	262093.29	416164.80
S7	123.05	481.66	604.71	S30	43458.13	262093.29	305551.41
S8	496.40	263.21	759.61	S31	90844.24	262093.29	352937.53
S9	12793.30	263.21	13056.51	S32	2132.08	264421.11	266553.19
S10	0.00	490355.28	490355.28	S33	1730.08	41237.84	42967.93
S11	34680.85	490355.28	525036.12	S34	1773.31	39873.65	41646.96
S13	48658.45	327702.66	376361.12	S35	2448.91	271.69	2720.60
S14	37.27	327702.66	327739.94	S36	75.74	8.40	84.14
S15	967116.87	3317567.74	4284684.61	S37	2524.64	280.09	2804.74
S16	230550.87	3317567.74	3548118.62	S38	203.99	223145.16	223349.16
S17	0.00	0.00	0.00	S39	15.09	1317.68	1332.78
S18	314.36	0.00	314.36	S40	267.54	224441.80	224709.33
S20	299.74	633.85	933.59	S41	7957.82	224441.80	232399.62
S21	230540.44	3317040.58	3547581.02	S42	16561.78	280.09	16841.87
S22	380684.86	3317040.58	3697725.44	S43	3816.77	229124.77	232941.54

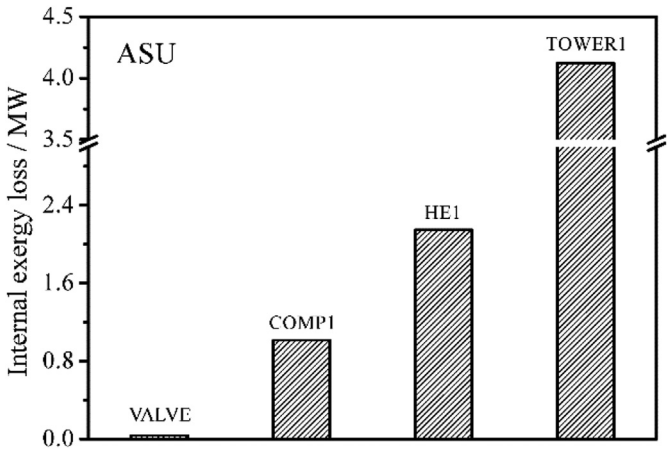

Fig. 6. Internal exergy loss in the blocks in ASU.

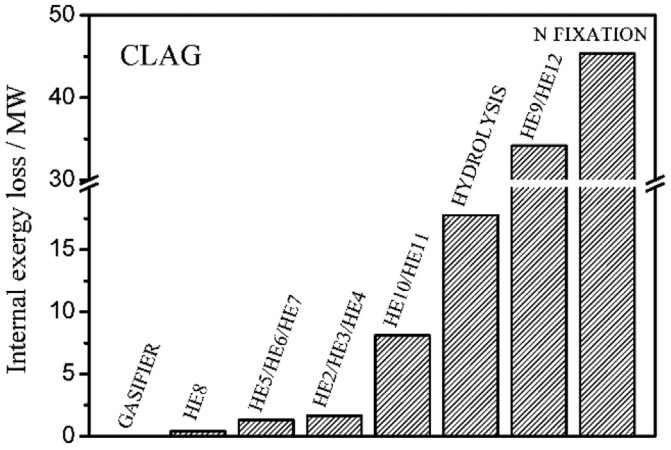

Fig. 7. Internal exergy loss in the blocks in CLAG unit.

Compared to the other two units (as shown in Figs. 7 and 8), the total internal exergy loss in ASU is quite low, accounting only for 4.3% of the total internal exergy loss of the system. This does not mean that the exergy efficiency of the CPU is very high. In fact, it is only about 15.7%. The main reason is that the exergy included in this unit is much less than those of the other two units. This result also indicates that, compared to the other two units, there is less capacity in the ASU to improve the overall exergy efficiency of the entire system.

Fig. 7 presents the internal exergy loss of each part of the CLAG unit. The N_2 fixation reactor experiences the largest internal exergy loss, followed by the heat exchanger HE9/HE11, the hydrolysis reactor, other heat exchangers, and the gasifier (in that order). The largest internal exergy loss in the N_2 fixation reactor is a result of the N_2 fixation reaction, and the internal exergy loss in HE9/HE12 is due to heat exchange with a large temperature difference.

Fig. 8 shows the internal exergy loss of each part of the CPU. The internal exergy loss of COMP2 is the largest, followed by those of HE13 and TOWER2, and the ABSORBER has the lowest exergy loss. The largest exergy loss occurring in COMP2 is mainly due to the large pressure difference between the inlet and outlet. The exergy loss in HE13 is ascribed to heat exchange with a large temperature difference between steam (condensed to liquid water) and ammonia water. The exergy loss in TOWER2 originates from the phase transformation of the liquid water to steam in the kettle reboiler of this tower.

The distribution of the fuel exergy conversion is shown in Fig. 9.

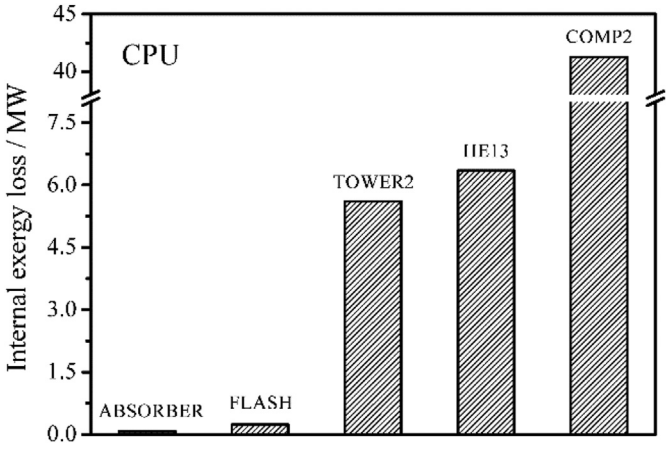

Fig. 8. Internal exergy loss in the blocks in CPU.

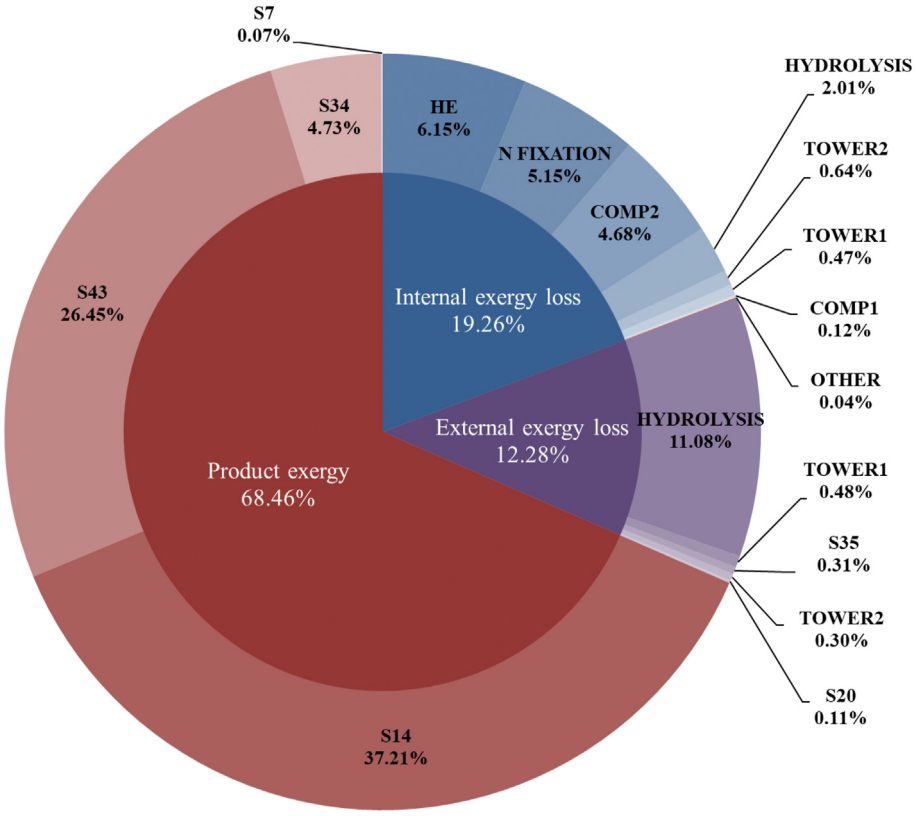

Fig. 9. The distribution of the fuel exergy conversion in the CLAG system.

It can be seen that the internal and external exergy losses account for 19.26% and 12.28% of the total fuel exergy, respectively. If NH_3 is taken as the only product of the system, the exergy efficiency of the system is 26.45%. But if the high purity O_2 and syngas (H_2 and CO) are also taken as the product, the exergy efficiency of the system reaches 68.46%. The exergy is mainly lost in heat exchangers, reactors, and pumps. Because of the limitations of the reaction conditions, the room for improvement is small for the reactors and pumps. However, there are many heat exchangers in the system. By optimizing the heat exchanger network, it is expected that the internal exergy loss of the system can be reduced significantly. Moreover, the external exergy loss caused by heat dissipation in the hydrolysis reactor can also be reduced by heat recovery.

3.5. Exergy cost analysis

The exergy analysis above allowed us to allocate and quantify the irreversibility and efficiency of the system. However, this analysis is insufficient for achieving energy reduction because the exergy analysis cannot identify the real causes of additional resource consumption [28,29]. In fact, to find out the real causes of economic losses, the relationship between the components in the system should be considered comprehensively. Exergy cost analysis, which is based on the structural theory of thermoeconomics, can be used to describe the interactions between components and quantify the thermodynamic cost formation of each stream according to irreversibility [30,31].

Based on the function of each component, the fuel–product definition is first implemented to determine the following productive structure. Generally, the exergy resource that is from other components or the environment can be regarded as "fuel," and the expected useful exergy can be regarded as "product." For a multistream heat exchanger, the exergy difference between the inlet and outlet streams for supplying heat is the fuel, whereas the exergy difference for the two cold streams is the product [32,33]. With respect to the compressor, fuel is the work provided by the environment, whereas the product is the exergy difference between the outlet stream and inlet stream [28,33]. For the tower, flash tank, and reactor, the fuel is the exergy contained in the inlet stream and the absorbed heat, whereas the product is the exergy contained in the outlet stream and the released heat. The fuels and products for all components in the CLAG system are listed in Table 5.

The productive structure diagram [33,34] of the CLAG system is

Table 5
Fuel–product definition for all components in the CLAG system.

No.	Component	Fuel	Product
1	COMP1	$F_1 = W_1$	$P_1 = E_{S2} - E_{S1}$
2	TOWER1	$F_3 = E_{S3} + H_1$	$P_3 = E_{S4} + E_{S5} + H_2$
3	HE1	$F_2 = E_{S6} - E_{S7} + E_{S4} - E_{S8}$	$P_2 = E_{S3} - E_{S2}$
4	VALVE	$F_4 = E_{S5}$	$P_4 = E_{S6}$
5	N FIX	$F_6 = E_{S11} + E_{S9} + E_{S28} + H_3$	$P_6 = E_{S13} + E_{S15}$
6	HE2	$F_5 = E_{S13} - E_{S14}$	$P_5 = E_{S9} - E_{S8} + E_{S11} - E_{S10}$
7	HE5	$F_7 = E_{S15} - E_{S16}$	$P_7 = E_{S22} - E_{S21} + E_{S28} - E_{S27}$
8	GASIF	$F_9 = E_{S18} + E_{S16} + H_4$	$P_9 = E_{S20} + E_{S21}$
9	HE8	$F_8 = E_{S17} + H_5$	$P_8 = E_{S18}$
10	HYDRO	$F_{10} = E_{S22} + E_{S25}$	$P_{10} = E_{S27} + E_{S29} + H6$
11	HE11	$F_{11} = E_{S29} - E_{S30}$	$P_{11} = E_{S25} - E_{S24}$
12	COMP2	$F_{12} = W_2$	$P_{12} = E_{S31} - E_{S30}$
13	HE12	$F_{13} = E_{S31} - E_{S32}$	$P_{13} = E_{S24} - E_{S23}$
14	FLASH	$F_{14} = E_{S32}$	$P_{14} = E_{S33} + E_{S38}$
15	ABSOR	$F_{15} = E_{S33} + E_{S36}$	$P_{15} = E_{S34} + E_{S39}$
16	TOWER2	$F_{17} = E_{S41} + H7$	$P_{17} = E_{S43} + E_{S42} + H8$
17	HE13	$F_{16} = E_{S42} - E_{S36} - E_{S35}$	$P_{16} = E_{S41} - E_{S38} - E_{S39}$

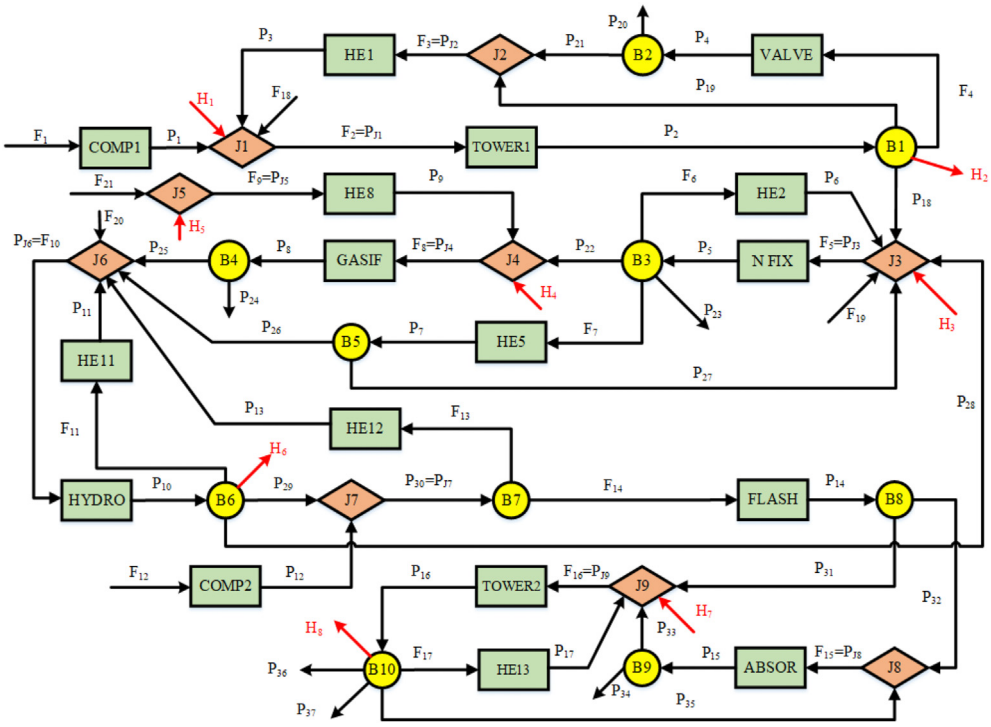

Fig. 10. Productive structure of the CLAG system.

shown in Fig. 10. Rectangles represent a component of a physical device, rhombi illustrate an aggregator of the fuel at the front of a downstream component, and circles indicate a splitter to divide a product into several streams to different ends. Fuel, product, and heat exergy, as the connections between the components, are represented "F," "P," and "H", respectively. It can be seen that the productive structure is significantly different from the physical structure shown in Fig. 2, especially in the structure of heat exchangers. More specifically, HE2, HE3, and HE4 in the physical structure are assembled into HE2 in the productive structure because they are equivalent to a heat exchanger from a functional perspective in this study. Correspondingly, HE5, HE6, and HE7 are assembled into HE5; HE10 and HE11 are assembled into HE11; HE9 and HE12 are assembled into HE12.

To determine the exergy cost distribution, the distribution coefficients, y_{ij}, are introduced, which quantify the part of the product of the jth component that becomes fuel of the ith component:

$$y_{ij} = \frac{E_{ji}}{P_j} \tag{13}$$

where E_{ji} is the exergy flow that represents the product of the jth component used as fuel of the ith component. Table S7 shows the values of E_{ji}. In this table, each row shows how the product of a given component becomes part of the fuel of other components or part of the system outlet, and each column corresponds to the fuel of a component, which comes either from other components or from the environment (represented by component 0). The summation by rows is the total product of the component, whereas the summation by columns represents the total fuel.

Once y_{ij} is calculated, the vector containing the exergy cost of each component can be calculated using Eq. (14).

$$\mathbf{P}^* = \mathbf{P} + (\mathbf{U_D} - \langle \mathbf{FP} \rangle)^{-1}\mathbf{I} \tag{14}$$

where **FP** is an $(n \times n)$ matrix containing elements y_{ij}, $\mathbf{U_D}$ is the $(n \times n)$ identity matrix, **P** is the $(n \times 1)$ product vector, and **I** is the $(n \times 1)$ irreversibility vector. The elements in the product vector are defined in Table 5, and the irreversibility vector is the difference between the product vector and fuel vector, i.e., **P**−**F**. Note that Eq. (14) also represents the decomposition of the exergy cost of each component by considering the irreversibility of other components [34–36].

The unit exergy cost of one component can be calculated by dividing the exergy cost of this component by the product exergy of the same component. The calculation results are shown in Table S8 (and also in Fig. 11).

Fig. 11 shows the processes of formation of the unit exergy costs of all components. It can be seen that the costs of components located at the beginning of the productive chain are smaller than those located at the end of this chain. In fact, each component is affected not only by its own irreversibility but also by the irreversibility of their upstream components in the productive chain. This understanding is clearly reflected in this figure. For example, the bars of the COMP1, HE8, and COMP2 are filled by only one color, which indicates that their unit exergy costs are only affected by their own irreversibility because they do not have an upstream component. In contrast, the other bars are filled with more than two colors. It is worth mentioning that HE13 can be affected by the irreversibility of all components in the system. Therefore, the bar contains all the colors.

From this figure, it can also be seen that the irreversibility of some components, such as ABSOR, FLASH, GASIF, and HE5, contribute little to the formation of their own unit exergy costs, as well as those of other components. However, the irreversibility of TOWER1 has a significant impact not only on itself but also on HE1 and VALVE. The irreversibility of N FIX is the main source of the unit exergy cost formation of some components, for example, HE2, HE5, GASIF, and HYDRO. As for the components of FLASH, ABSOR, and TOWER2, the most relevant contribution to their cost formation is

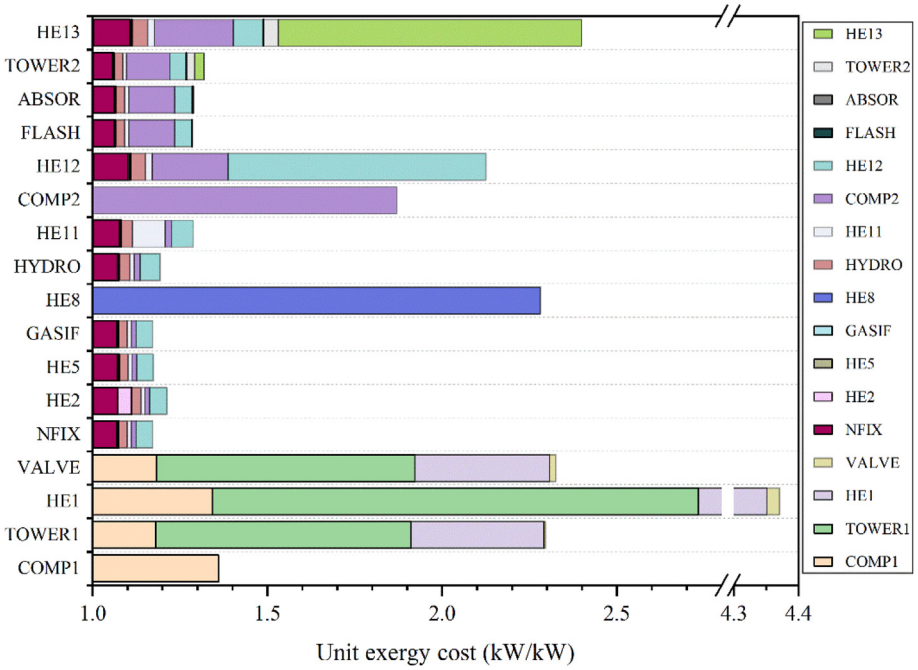

Fig. 11. Formation of the unit exergy costs of the CLAG system.

the irreversibility of COMP2. Considering the above results, the optimization of the CLAG system should focus on the optimization of TOWER1, N FIX, and COMP2 because of the significant effects of their irreversibility on other components.

In addition, the unit exergy cost of HE1 (in ASU), which is up to 4.35, is much higher than that of the other components. In the CLAG unit, the maximum unit exergy cost comes from the heat exchanger HE8. In the CPU, the unit exergy costs of the heat exchangers HE12 and HE13 are greater than those of other components. The most relevant contributions to the cost formation of the above components are all the irreversibility of their own. The much higher exergy cost of HE1 is due to not only its high fuel exergy cost but also its high exergy loss. The high exergy loss in HE1 is mainly due to heat exchange with high temperature differences and phase transformation. For HE8, the energy penalty for water vaporization results in great thermodynamic irreversibility to this component, which is the main reason for its high unit exergy costs. For HE12 and HE13, the high unit exergy costs are mainly due to the H_2O vaporization in HE12 and steam condensation in HE13. It can be seen that the components with high unit exergy costs are the heat exchangers with a phase transformation process. In the current system, to reduce the unit exergy cost, heat integration should be considered carefully.

4. Conclusions

In this work, a CLAG system model with a capacity of 300,000 t/a was first established in Aspen Plus. Based on the established model, sensitivity analysis of the key operating parameters was conducted to obtain the optimal operating conditions. Then, exergy analysis over the CLAG system under the optimal operating condition was carried out to calculate the exergy efficiency of the system and to discover the distribution of exergy loss in the system. Finally, to understand the cost formation process, exergy cost analysis was conducted. The main conclusions are as follows:

(1) The established system model consists of three units: ASU, CLAG, and CPU. The kinetics-based MFR model was used to simulate the N_2 fixation and hydrolysis reactors. The kinetics obtained from the literature was imported into Aspen Plus.
(2) The optimal operating conditions were N_2 fixation reactor temperature of 1700 °C, hydrolysis reactor temperature of 1000 °C, air flow rate of 2227 kmol/h, and the H_2O flow rate of 20000 kmol/h.
(3) The internal and external exergy losses account for about 19% and 12% of the total fuel exergy, respectively. Exergy is mainly lost in heat exchangers, reactors, and pumps. If NH_3 is taken as the only product of the system, the exergy efficiency of the system is about 26%. But, if the high purity O_2 and syngas are also taken as the products, the exergy efficiency of the system reaches to 68%.
(4) The unit exergy cost of the heat exchangers is larger than that of the other components and the irreversibility of TOWER1, N FIX, and COMP2 have a great influence on the formation of the exergy cost of other components.

We note that there is a big gap between the above theoretical analyses and the technical practice, as there contains a high level of uncertainty on technical viability to make extrapolation from TGA to 300000 t/y unit, especially under such extreme temperature conditions. There also has much space for the optimization of the proposed CLAG system. As for the design of the large scale reactor + cyclone system, we think the blast furnace for ironmaking in metallurgical industry is a useful reference, and the blast furnace in essence is a moving bed. The heat supplied to the blast furnace is from the combustion of part of coke. The nitrogen fixation reactor in the CLAG system can also be heated by fuel combustion, but the combustion products should not be directly mixed with the gas in the reactor. Therefore, ceramic pipelines can be used in which fuel is combusted to isolate the atmospheres and supply the huge amount of heat. Another improvement aspect is to consider the impurities of the raw materials, for example, Ar should be taken into account when describing air composition and “carbon” should not be taken as pure graphite.

Declaration of competing interest

The authors declare that they have no known competing financial interests or personal relationships that could have appeared to influence the work reported in this paper.

Acknowledgements

This work was supported by “National Key R&D Program of China (2018YFB0605403)” and “National Natural Science Foundation of China (52025063)”.

Appendix A. Supplementary data

Supplementary data to this article can be found online at https://doi.org/10.1016/j.energy.2021.120767.

Credit author statement

Xiaoyu Wang: Conceptualization, Data curation, Formal analysis, Investigation, Methodology, Software, Validation, Visualization, Writing – original draft, Writing – review & editing. Mingze Su: Conceptualization, Data curation, Formal analysis, Investigation, Methodology, Writing – review & editing. Haibo Zhao: Conceptualization, Funding acquisition, Methodology, Project administration, Resources, Supervision, Writing – review & editing.

References

[1] Rafiqul I, Weber C, Lehmann B, et al. Energy efficiency improvements in ammonia production-perspectives and uncertainties. Energy 2005;30:2487–504.
[2] Wu Y, Jiang G, Zhang H, et al. Fe_2O_3, a cost effective and environmentally friendly catalyst for the generation of NH_3-a future fuel-using a new Al_2O_3-looping based technology. Chem Commun 2017;53:10664–7.
[3] Guo J, Chen P. Catalyst: NH_3 as an energy carrier. Chem 2017;3:709–12.
[4] Lamb KE, Dolan MD, Kennedy DF. Ammonia for hydrogen storage; A review of catalytic ammonia decomposition and hydrogen separation and purification. Int J Hydrogen Energy 2019;44:3580–93.
[5] Gálvez ME, Halmann M, Steinfeld A. Ammonia production via a two-step Al_2O_3/AlN thermochemical cycle. 1. Thermodynamic, environmental, and economic analyses. Ind Eng Chem Res 2007;46:2042–6.
[6] Heidlage MG, Kezar EA, Snow KC, et al. Thermochemical synthesis of ammonia and syngas from natural gas at atmospheric pressure. Ind Eng Chem Res 2017;56:14014–24.
[7] Wang Q, Guo J, Chen P. Recent progress towards mild-condition ammonia synthesis. J Energy Chem 2019;36:25–36.
[8] Adanez J, Abad A, Garcia-Labiano F, et al. Progress in chemi- cal-looping combustion and reforming technologies. Prog Energy Combust 2012;38:215–82.
[9] Adanez J, Abad A, Mendiara T, et al. Chemical looping combustion of solid fuels. Prog Energy Combust 2018;65:6–66.
[10] Zhao H, Tian X, Ma J, et al. Development of tailor-made oxygen carriers and reactors for chemical looping processes at Huazhong University of Science & Technology. Int J Greenh Gas Control 2020;93:102898.
[11] Richter HJ, Knoche KF. Efficiency and costing. Am Chem Soc 1983;235:71–85.
[12] Ishida M, Zheng D, Akehata T. Evaluation of a chemical-looping-combustion power-generation system by graphic exergy analysis. Energy 1987;12:147–54.
[13] Gálvez ME, Frei A, Halmann M, et al. Ammonia production via a two-step Al_2O_3/AlN thermochemical cycle. 2. Kinetic analysis. Ind Eng Chem Res 2007;46:2047–53.
[14] Gao Y, Wu Y, Zhang Q, et al. N-desorption or NH_3 generation of TiO_2-loaded Al-based nitrogen carrier during chemical looping ammonia generation technology. Int J Hydrogen Energy 2018;43:16589–97.
[15] Gálvez ME, Hischier I, Frei A, et al. Ammonia production via a two-step Al_2O_3/AlN thermochemical cycle. 3. influence of the carbon reducing agent and cyclability. Ind Eng Chem Res 2008;47:2231–7.
[16] Zhang Q, Wu Y, Gao Y, et al. High-performance mesoporous (AlN/Al_2O_3) for enhanced NH_3 yield during chemical looping ammonia generation technology. Int J Hydrogen Energy 2020;45:9903–13.
[17] Wu Y, Gao Y, Zhang Q, et al. Promising zirconia-mixed Al-based nitrogen carriers for chemical looping of NH_3: reduced NH_3 decomposition and improved NH_3 yield. Fuel 2020;264:116821.
[18] Michalsky R, Pfromm PH. Chromium as reactant for solar thermochemical synthesis of ammonia from steam, nitrogen, and biomass at atmospheric pressure. Sol Energy 2011;85:2642–54.
[19] McEnaney JM, Singh AR, Schwalbe JA, et al. Ammonia synthesis from N_2 and H_2O using a lithium cycling electrification strategy at atmospheric pressure. Energy Environ Sci 2017;10:1621–30.
[20] Michalsky R, Avram AM, Peterson BA, et al. Chemical looping of metal nitride catalysts: low-pressure ammonia synthesis for energy storage. Chem Sci 2015;6:3965–74.
[21] Laassiri S, Zeinalipour-Yazdi CD, Catlow CRA, et al. The potential of manganese nitride based materials as nitrogen transfer reagents for nitrogen chemical looping. Appl Catal B Environ 2018;223:60–6.
[22] Gao W, Guo J, Wang P, et al. Production of ammonia via a chemical looping process based on metal imides as nitrogen carriers. Nat Energy 2018;3:1067–75.
[23] Ranzi E, Frassoldati A, Grana R, et al. Hierarchical and comparative kinetic modeling of laminar flame speeds of hydrocarbon and oxygenated fuels. Prog Energ Combust 2012;38:468–501.
[24] Mahalatkar K, Kuhlman J, Huckaby ED, et al. Computational fluid dynamic simulations of chemical looping fuel reactors utilizing gaseous fuels. Chem Eng Sci 2011;66:469–79.
[25] Su M, Zhao H, Ma J. Computational fluid dynamics simulation for chemical looping combustion of coal in a dual circulation fluidized bed. Energy Convers Manag 2015;105:1–12.
[26] Xiong J, Zhao H, Zheng C. Exergy analysis of a 600 MWe oxy-combustion pulverized-coal-fired power plant. Energy Fuel 2011;25:3854–64.
[27] Niasar MS, Amidpour M. Conceptual design and exergy analysis of an integrated structure of natural gas liquefaction and production of liquid fuels from natural gas using Fischer-Tropsch synthesis. Cryogenics 2018;89:29–41.
[28] Xiong J, Zhao H, Zhang C, Zheng C, Luh PB. Thermoeconomic operation optimization of a coal-fired power plant. Energy 2012;42:486–96.
[29] Zhang C, Wang Y, Zheng C, Lou X. Exergy cost analysis of a coal fired power plant based on structural theory of thermoeconomics. Energy Convers Manag 2006;47:817–43.
[30] Torres C. Symbolic thermoeconomic analysis of energy systems. In: Frangopoulos CA, editor. Exergy, energy system analysis and optimization, from Encyclopedia of life support systems (EOLSS). Oxford: EOLSS Publishers; 2006.
[31] Erlach B, Serra L, Valero A. Structural theory as standard for thermoeconomics. Energy Convers Manag 1999;40:1627–49.
[32] Jin B, Zhao H, Zheng C. Thermoeconomic cost analysis of CO_2 compression and purification unit in oxy-combustion power plants. Energy Convers Manag 2015;106:53–60.
[33] Jin B, Zhao Y, Fan Y, Deng Z, Liang Z. Thermal management for chemical looping systems with chemical production. Chem Eng Sci 2020;214:115431.
[34] Usón S, Uche J, Martínez A, Amo A, Acevedo L, Bayod A. Exergy assessment and exergy cost analysis of a renewable-based and hybrid trigeneration scheme for domestic water and energy supply. Energy 2019;168:662–83.
[35] Torres C, Valero A, Rangel V, Zaleta A. On the cost formation process of the residues. Energy 2008;33:144–52.
[36] Usón S, Valero A, Agudelo A. Thermoeconomics and industrial symbiosis. Effect of by-product integration in cost assessment. Energy 2012;45:43–51.